Soft Matter

Direct Measurements & Simplified Models of Colloidal Interactions & Diffusion with Adsorbed Macromolecules

Journal:	*Soft Matter*
Manuscript ID	SM-ART-05-2024-000662.R2
Article Type:	Paper
Date Submitted by the Author:	01-Aug-2024
Complete List of Authors:	Ellingson, Mikael; Johns Hopkins University Bevan, Michael; Johns Hopkins University,

Direct Measurements & Simplified Models of Colloidal Interactions & Diffusion with Adsorbed Macromolecules

Mikael O. Ellingson and Michael A. Bevan†
Chemical & Biomolecular Engr., Johns Hopkins Univ., Baltimore, MD 21218

Abstract

We report total internal reflection microscopy measurements of 3D trajectories of ensembles of micron sized colloidal particles near interfaces with and without adsorbed macromolecules. Evanescent wave scattering reveals nanometer scale motion normal to planar surfaces and sub-diffraction limit lateral motion is resolved via image analysis. Equilibrium and non-equilibrium analyses of particle trajectories reveal self-consistent position dependent energies (energy landscapes) and position dependent diffusivities (diffusivity landscapes) both perpendicular and parallel to interfaces. For bare colloids and surfaces, electrostatic and hydrodynamic interactions are accurately quantified with established analytical theories. For colloids and surfaces with adsorbed macromolecules, conservative forces are accurately quantified with models for interactions between brush layers, whereas directly measured position dependent diffusivities require novel models of spatially varying permeability within adsorbed layers. Agreement between spatially resolved interactions and diffusivities and rigorous simplified models provide a basis to consistently interpret, predict, and design colloidal transport in the presence of adsorbed macromolecules for diverse applications.

keywords: polymer brush interactions | polymer brush permeability | hydrodynamic interactions | lubrication | adsorbed mucin | total internal reflection microscopy

Introduction

Colloidal interactions and dynamics near interfaces are ubiquitous in numerous problems in science and technology involving diverse natural and synthetic materials. For example, colloids deposit onto surface in printing,[1] assemble into complex microstructures on substrates for functional coatings,[2] transport through porous media in the environment,[3] and permeate biological barriers in biomedical applications.[4] In many such applications, colloidal interactions and diffusion are significantly influenced by interfacial macromolecules (*e.g.*, polymer, protein, natural organic matter, mucus, extra-cellular matrix, glycocalyx, etc.) by altering both conservative forces (*e.g.*, steric repulsion) and non-conservative forces (*e.g.*, hydrodynamics). To understand, design, and control interfacial colloidal systems, it is essential to have accurate first principles models validated by high fidelity measurements for interactions, diffusion, and their coupling for both bare and macromolecule coated surfaces.

It is well known that colloidal particle interactions with interfaces can be modelled as the superposition of electrostatic, van der Waals, and macromolecular contributions.[5] Such interactions correspond to conservative forces due to spatial gradients in the separation dependent free energy between colloids and surfaces (*i.e.,* energy landscapes). In addition, the squeezing flow of viscous fluids between colloids and surfaces produces hydrodynamic interactions[6-7] that produce position dependent colloidal diffusivities (*i.e.,* diffusivity landscapes). The energy and diffusivity landscapes determine the equilibrium and dynamic behavior of colloids near interfaces. The Boltzmann equation captures equilibrium position distributions based on interfacial energy

† To whom correspondence should be addressed. email: mabevan@jhu.edu

landscapes, and the Smoluchowski equation quantifies dynamic processes (*e.g.*, deposition, adsorption, assembly, etc.) based on the combined roles of energy and diffusivity landscapes.[8-9]

Many studies have mechanically probed surface forces between bare and polymer coated surfaces.[10-11] Such mechanical measures report separation dependent conservative steric forces (osmotic, elastic repulsion) and, in some cases, non-conservative hydrodynamic forces (lubrication) to estimate polymer permeability.[12-18] Results have shown good agreement with established theories in the strong compression limit (strong forces, small separations). However, strong compression in mechanical measurements significantly deforms layers compared to near-equilibrium layer deformations encountered during kT-scale collisions for Brownian colloids. Mechanical probes are also not torque free as in kT-scale collisions between colloids free to undergo coupled Brownian translation and rotation. Average polymer hydrodynamic properties (effective thickness, viscosity, no-slip boundary, etc.) have been inferred by fitting lubrication models to measured hydrodynamic forces. However, such measurements do not spatially resolve hydrodynamic interactions via model-free analyses, which limits direct translation of such measures to position dependent diffusivities of polymer coated colloids.

Analyzing colloidal trajectories near surfaces has been used to non-intrusively obtain colloidal interactions and diffusivities. Total Internal Reflection Microscopy (TIRM)[19-20] tracks 3D super-resolution trajectories of colloidal particles diffusing and interacting on surfaces.[21-22] Such studies generally report average lateral or normal diffusivities via mean squared displacements or autocorrelation functions.[23-24] More recently, methods have been developed to spatially resolve position dependent diffusivities by fitting the Smoluchowski equation coefficients to measured trajectory data,[8-9] which have been applied to analyze bare[25-28] and polymer coated colloids.[9, 29] However, beyond this handful of measurements, few studies report such analyses of directly measured colloidal trajectories to yield both energy and diffusivity landscapes. We are unaware of any reports of a consistent analysis of 3D interfacial colloidal trajectories in terms of both normal and lateral energy and diffusivity landscapes for polymer coated colloids.

Simple models of interactions between polymer coated colloids are less well established than models of bare colloidal interactions (*i.e.*, van der Waals, electrostatics).[5, 10] Conservative forces between polymer layers depend on adsorbed amount, solvent quality, and compression extent, which determine polymer concentration profiles and free energy contributions (elastic, osmotic). Polymer brush interactions in good solvents are perhaps the most studied, where analytical models[30-32] of varying complexity show approximate agreement with directly measured interactions. However, assessing agreement between models and experiments is limited by various sources of uncertainty including measurement resolution, independent model parameter estimation, and correspondence between model assumptions and realistic experimental systems.[33]

Open questions remain about how to model hydrodynamic interactions between polymer coated colloids and their role in determining position dependent colloidal diffusivities. Theoretical separation dependent mobility coefficients for spherical particle motion perpendicular or parallel to plane walls were reported over fifty years ago,[6-7] and such models have been extended to include multibody hydrodynamic interactions in concentrated interfacial colloidal ensembles.[34] However, for interfacial lubrication in the presence of permeable polymers brushes, modeling efforts have been limited in number and rigor. For example, coarse grained computer simulations[35-36] without realistic molecular potentials, particularly for aqueous polymers,[37-38] do not yield analytical models or capture long range hydrodynamic interactions consistent with continuum fluid mechanics. Treatment of permeable brushes in the lubrication limit has been applied to limited conditions of

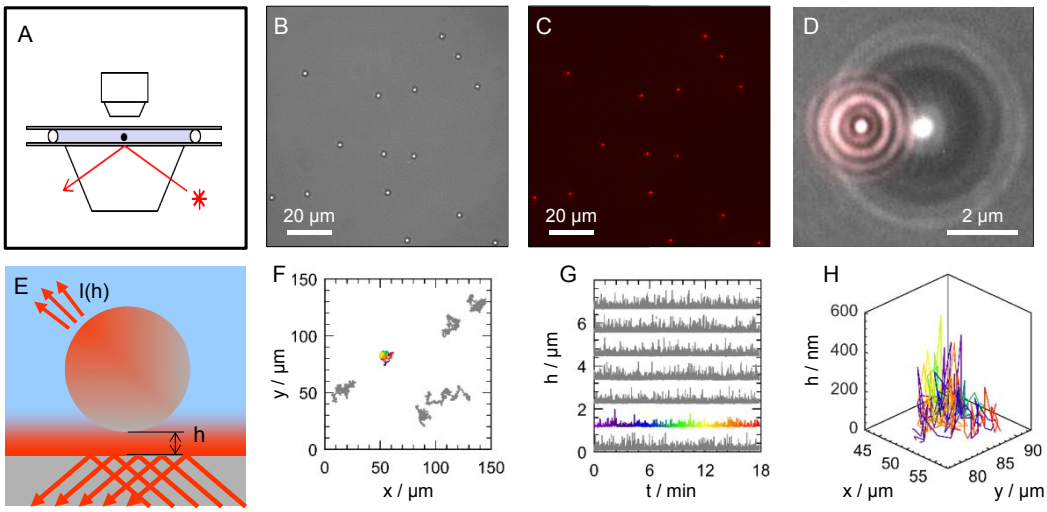

Fig. 1. Ensemble total internal reflection microscopy (TIRM). (A) Schematic of microscopy setup with laser path for evanescent wave generation (not to scale). Ensemble of 2μm silica particles with, (B) transmitted light and (C) evanescent wave illumination. (D) Single particle scattering evanescent wave.[42] (E) Schematic view of single particle scattering evanescent wave showing exponential scale to height, h, as $I(h)=I_0\exp(-\beta h)$, which enables nanometer scale height resolution.[19] Ensemble of (F) lateral and (G) normal trajectories. (H) Single 3D super-resolution trajectory (colored by time, same particle as in F, G).

highly compressed, low permeability, uniform density brushes[39-40] or treated more rigorously to yield complex results with parameters that are difficult to independently evaluate[41] (although spatially resolved colloidal diffusivities[9, 29] suggest the validity of this latter model). Overall, there are significant limitations of current models for hydrodynamic interactions between polymer coated colloids and surfaces and their position dependent diffusivity. Development of more refined models is perhaps limited by the number of direct measurements.

Here, we report measurements of 3D colloidal trajectories near surfaces (**Fig. 1**), with and without polymers, which we use to evaluate models for position dependent colloidal interactions and diffusivities, both normal and parallel to planar surfaces. We use Total internal reflection microscopy (TIRM) to monitor sub-diffraction limit 3D trajectories in dilute ensembles of micron scale colloids[21] either electrostatically stabilized above a bare microscope slide or sterically stabilized via symmetric PEG brush interactions or asymmetric PEG brush-adsorbed mucin interactions. Each particle's 3D trajectory is analyzed via equilibrium analysis to obtain interactions normal to underlying planar surfaces, and dynamic analyses of the same trajectories are used to measure position dependent diffusivities normal to the wall and average lateral diffusivities. Results are compared with rigorous but simplified theories for electrostatic, van der Waals, steric, and hydrodynamic interactions to develop a complete and consistent understanding of how adsorbed polymers modify all interactions between particles and surfaces.

Theory

Potential Energy Profiles

The net potential energy for a spherical colloidal particle near a planar surface (**Fig. 2**) can be expressed by the superposition of contributing potentials as,

$$U(h)=U_G(h)+U_E(h)+U_V(h)+U_S(h) \quad (1)$$

where the subscripts refer to the gravitational (G), electrostatic (E), van der Waals (V), and polymer

steric (S) interactions, and h is the particle surface to wall surface separation. The gravitational potential energy of each particle depends on its buoyant weight, G, as,

$$U_G(h) = Gh = mgh = \pi a^3(\rho_p - \rho_f)gh \tag{2}$$

where m is buoyant mass, g is acceleration due to gravity, a is particle radius, and ρ_p and ρ_f are particle and fluid densities. The electrostatic potential energy of charged colloidal particles interacting with a charged surface in electrolyte solutions is given by superposition of the non-linear Poison-Boltzmann solution of electrostatic double layer on flat plates[5] with the Derjaguin approximation[43] to correct for the sphere-wall interactions[44] as,

$$\begin{aligned} U_E(h) &= 2\pi a \int_h^\infty B' \kappa N_A C \exp(-\kappa l)\, dl = Ba \exp(-\kappa h) \\ B &= 64\pi\varepsilon \left(\frac{kT}{e}\right)^2 \tanh\left(\frac{e\psi_p}{4kT}\right)\tanh\left(\frac{e\psi_w}{4kT}\right), \quad \kappa = \left[\frac{2e^2 N_A C}{\varepsilon kT}\right]^{1/2} \end{aligned} \tag{3}$$

where κ^{-1} is the Debye length, k is Boltzmann's constant, T is absolute temperature, ε is the solvent dielectric constant, e is elemental charge, ψ_p and ψ_w are particle and wall surface potentials, N_A is

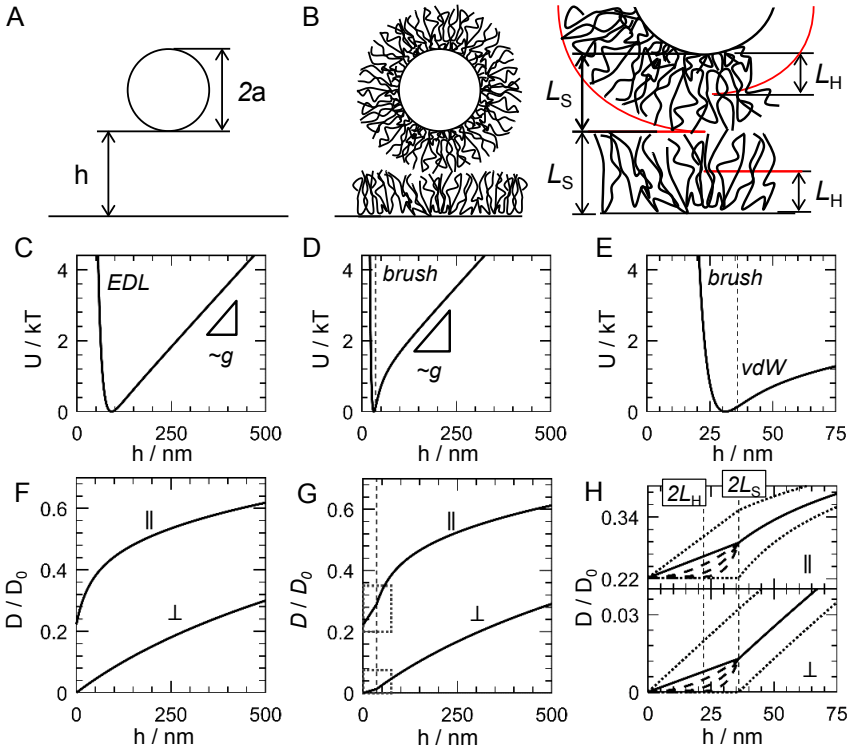

Fig. 2. Energy & diffusivity landscapes for bare and polymer coated colloids and wall surface. (A) Bare particle of diameter, $2a$, with separation, h, from wall surface. (B) Same as panel A, except steric, L_S, and hydrodynamic, L_H, thicknesses indicated on polymer brush. Energy landscapes (potential energy profiles) from Eq. (1) for (C) bare particles with electrostatic repulsion and gravity, (D) polymer coated particles with steric, van der Waals, and gravity, and (E) shorter separation view of steric and van der Waals interactions. Diffusivity landscapes (elevation dependent diffusivity, Eqs. (8)-(13)) perpendicular and parallel to a wall for (F) bare particles and walls, (G) polymer coated particles and walls, and (H) short separation view showing tunable position dependent diffusivity between completely permeable/impermeable limits. Vertical dashed lines indicate $2L_H$ and $2L_S$.

Avogadro's number, C is the electrolyte molarity, and $B'=B(2\pi\varepsilon e/kT)^{-1}$. This expression is simplified for unit valence electrolyte and valid for thin double layers compared to sphere radius ($\kappa a>>1$) and particle-wall separations ($\kappa h<<1$). The van der Waals potential energy of a colloidal particle interacting with a planar surface is given for flat plates by the Lifshitz theory[45] and the Derjaguin approximation[46] to correct for the sphere-wall interactions as,[42]

$$U_V(h) = 2\pi a \int_h^\infty \frac{A(l)}{12\pi l^2} dl \approx -\left(Aa/6\right) h^{-p} \tag{4}$$

where $A(l)$ is the Hamaker function between half spaces,[45] and p and A are values in a power law potential fit to the rigorous expression over separation ranges of interest,[21, 25] including in the presence of adsorbed polymers in good solvents.[47-48]

The steric potential between a polymer coated colloid and planar surface can be determined based on the separation dependent free energy change to compress polymer brushes between flat plates, and then using the Derjaguin approximation[49] for the sphere-wall geometry. For kT-scale Brownian collisions between polymer brushes, the interaction is determined by small compression at brush peripheries where density profiles vanish. The free energy of compressing a single brush with an approximately parabolic density profile is given by,[31]

$$\frac{f(\delta)}{f_0} = \frac{5}{9}\left[\left(\frac{\delta}{L_S}\right)^{-1} + \left(\frac{\delta}{L_S}\right)^{2} - \frac{1}{5}\left(\frac{\delta}{L_S}\right)^{5}\right] \approx 1 + c_1 \exp\left[-c_2 \frac{\delta}{L_S}\right] \tag{5}$$

where f_0 and f are the free energies of the uncompressed and compressed brushes, L_S and δ are the uncompressed and compressed brush thickness, and the right hand side with c_1=10, and c_2=112 accurately captures the complete expression to ~50% compression.[29, 50] Compression of two brushes in the Derjaguin approximation for the sphere-wall geometry[49] is then,

$$\begin{aligned} U_S(h) &= 2\pi a \int_h^{2L_S} 2\left[f\left(l/2\right) - f_0\right] dl = \frac{40\pi f_0 a L_S}{9}\left[-\ln\beta + \frac{9}{5}\beta - \frac{1}{3}\beta^3 + \frac{1}{30}\beta^6 - \frac{3}{2}\right] \\ &\approx \Gamma a \exp\left[-\gamma h\right], \quad \Gamma = 80\pi f_0 L_s, \quad \gamma = 17/3L_S \end{aligned} \tag{6}$$

where $\beta=h/2L_S$, and the simple exponential form accurately captures the full expression for up to 50% compression. For asymmetric layers, the same potential can be used with different interpretation of parameters,[29] where the prefactor involves both layers' uncompressed free energies and the contact height is the sum of the individual uncompressed layer dimensions.

Interfacial Colloidal Diffusion

The bulk single particle diffusivity is given by the Stokes-Einstein equation as,[51-52]

$$D_0 = \frac{kT}{6\pi\mu a} \tag{7}$$

where μ is the medium viscosity. For a single bare colloid near a bare planar surface (**Fig 2**), separation dependent hydrodynamic interactions modify the single particle diffusivity. For diffusion normal to a planar surface, the position dependent diffusivity is given by,[23-24]

$$D_\perp(h) = D_0 H_\perp(h) \tag{8}$$

where a rigorous analytical solution for the position dependent mobility[6] and a simple accurate Pade approximant[24] are given by,

$$H_{\perp}(h)=\left[\frac{4}{3}\sinh(\alpha)\sum_{n=1}^{\infty}\frac{n(n+1)}{(2n-1)(2n+3)}\left(\frac{2\sinh((2n+1)\alpha)+(2n+1)\sinh(2\alpha)}{4\sinh^2((n+1/2)\alpha)-(2n+1)^2\sinh^2(\alpha)}-1\right)\right]^{-1} \approx \frac{6(h/a)^2+2(h/a)}{6(h/a)^2+9(h/a)+2} \quad (9)$$

where $\alpha=\cosh^{-1}((2a+h)/a)$. For diffusion parallel to a planar surface, the elevation dependent diffusivity is given by,[34, 53]

$$D_{\mathsf{P}}(h)=D_0H_{\mathsf{P}}(h) \quad (10)$$

where a closed-form matched asymptotic expansion solution[53] that captures exact results at all separations (including lubrication[7] and long-range[54] asymptotic limits) and a simple accurate Pade approximant[24] are given by,

$$H_{\mathsf{P}}(h)=\begin{cases}1-\dfrac{15/8}{\ln(\omega-1)}-\exp[1.80359(\omega-1)]+0.319037(\omega-1)^{0.2592} & \omega\le 1.1\\ 1-\dfrac{9}{16}\omega^{-1}+\dfrac{1}{8}\omega^{-3}-\dfrac{45}{256}\omega^{-4}-\dfrac{1}{16}\omega^{-5}+0.22205\omega^{-6}-0.20521\omega^{-7} & \omega>1.1\end{cases} \approx \frac{234(h/a)^2+114(h/a)+2}{234(h/a)^2+241(h/a)+9} \quad (11)$$

where $\omega=(2a+h)/a$. For permeable polymer brushes (**Fig. 2**), a rigorous (and complex) solution to the lubrication equation inside and outside brushes[41] for normal motion modifies the bare particle mobility (Eq. (9)), where key features can be captured by a simple analytical form as,[9]

$$H_{\perp,P}(h,L_S,L_H,n)=\begin{cases}H_{\perp}(h)/k_{nc}(h) & h\ge 2L_S\\ H_{\perp}(h)/\left[k_{nc}(2L_S)+k_{c1}(h)+k_{c2}(h)\right] & h<2L_S\end{cases} \approx \begin{cases}H_{\perp}(h-2L_H) & h\ge 2L_S\\ H_{\perp}(2L_S-2L_H)[h/2L_S]^n & h<2L_S\end{cases} \quad (12)$$

where k_{nc}, k_{c1}, k_{c2} refer to position dependent corrections for uncompressed and compressed brushes, L_H is effective hydrodynamic brush thickness, and n effectively tunes layer permeability (n=1 is completely permeable, n=∞ is impermeable). We are unaware of hydrodynamic models for the torque free lateral motion of spherical particles on surfaces in the presence of adsorbed polymer layers (other than long range asymptotic behavior[55]). As a result, we assume a simple model for lateral motion that modifies the bare particle lateral mobility (Eq.(11)) in a manner analogous to Eq. (12) with the same parameters, differing only by an additive contact value, as,

$$H_{\mathsf{P},P}(h,L_S,L_H,n)=\begin{cases}H_{\mathsf{P}}(h-2L_H) & h\ge 2L_S\\ H_{\mathsf{P}}(2L_S-2L_H)[h/2L_S]^n+H_{\mathsf{P}}(0) & h<2L_S\end{cases} \quad (13)$$

Laterally diffusing interfacial colloids confined within normal energy wells (*i.e.*, Eq. (1)) have average lateral diffusivities given by,[34, 53]

$$\left\langle D_{\mathrm{P}} \right\rangle = \frac{\int D_{\mathrm{P}}(h)\, p(h) dh}{\int p(h) dh} \tag{14}$$

where $p(h)$ is the Boltzmann distribution of a colloid in an energy well, $U(h)$, given by,

$$p\left(h\right) = p(h_m) \exp\left[-\frac{U(h) - U(h_m)}{kT} \right] \tag{15}$$

where h_m is the most probable height at the potential energy minimum.

Particle Trajectory Analysis

Each particle's 3D trajectory (**Figs. 1, 2**) can be analyzed to obtain its position dependent potential and diffusivity. Many observations of each particle's time dependent elevation, $h(t)$, can be used to obtain a time averaged histogram of heights, $p(h)$, which can be inverted via Boltzmann's equation (Eq. (15)) to obtain each particle's potential energy profile as,[21]

$$U\left(h\right) - U\left(h_m\right) = kT \ln\left[p\left(h_m\right) / p\left(h\right) \right] \tag{16}$$

Each particle's time dependent trajectory, $x(t)$, $y(t)$, parallel to a planar surface can be analyzed as a mean squared displacement over multiple time origins in 2D, $\langle r^2 \rangle$ (where $r^2 = x^2 + y^2$), as,

$$\left\langle r^2 \right\rangle = \frac{1}{N} \sum_{i=1}^{N} \left[r\left(t + t_{0,i}\right) - r\left(t_{0,i}\right) \right]^2 \tag{17}$$

where N is the number of time origins. The slope of the mean square displacement vs. time provides the average lateral diffusion coefficients as,

$$\left\langle r^2 \right\rangle = 4 \left\langle D_{\mathrm{P}} \right\rangle t + \Delta^2 \tag{18}$$

where Δ^2 is related to the square of the uncertainty in the particle center location due to limited resolution in video microscopy measurements.[56-57]

In addition to the equilibrium analysis (Eq. (16)) of each particle's time dependent elevation, $h(t)$, a dynamic analysis[8-9] of the probability density evolution, $p(h,t)$, for each particle can be used to obtain the coefficients of the of the Smoluchowski equation as,

$$\frac{\partial p(h,t)}{\partial t} = \frac{\partial}{\partial h} D_{\perp}(h) \left[\frac{\partial p(h,t)}{\partial h} + \frac{p(h,t)}{kT} \frac{dU(h)}{dh} \right] \tag{19}$$

where each particle's normal position dependent diffusivity, $D_{\perp}(h)$, is obtained along with $U(h)$.

Materials & Methods

Materials. Nominal 2.34 μm diameter SiO_2 colloids (Bangs Laboratories) were used without modification, or modified with 1-octadecanol (Sigma-Aldrich) as previously described.[58] Glass microscope slides were sonicated in isopropanol for 30 min, sonicated in acetone for 30 min, immersed in Nochromix (Godax Laboratories) for 30 min, sonicated in 0.1 M KOH for 15 min, washed with DI water (18.3 MΩ/cm), and dried with nitrogen. For polymer experiments, slides were spin-coated at 3kRPM with a 3wt% solution of polystyrene (Sigma-Aldrich, 192 kDa) in toluene. Poly(ethylene glycol)−poly(propylene oxide)-poly(ethylene glycol) (PEG-PPO-PEG)

triblock copolymer (F108 Pluronic, BASF) with segment molecular weights of 5400/3300/5400 g/mol. The copolymer was dissolved in DI water at 1000 ppm and then adsorbed to the 1-octadecanol coated colloidal particles and polystyrene coated slides for a minimum of 2 h. Colloidal dispersions were washed with 150 mM NaCl three times to remove excess polymer. To functionalize with mucin, the same coating procedure was performed with 1mg/mL lyophilized bovine submaxillary mucin (Sigma) in 150 mM NaCl and 6 mM NaN_3 for a minimum of 4 hours.

Total Internal Reflection Microscopy. (TIRM). TIRM experiments were performed in sample cells consisting of 5 mm inside diameter Vinton O-rings (McMaster Carr) sealed between the microscope slide and a glass coverslip (Corning). A 15 mW 632.8 nm helium−neon laser (Melles Griot) and a 68° dovetail prism (Red Optronics) were used to generate an evanescent wave decay length of 114 nm. A 12-bit CCD camera (ORCA-ER, Hamamatsu, Japan) on an upright optical microscope (Zeiss Axio Imager A1m) with a 40× objective. CCD images were 204×155 μm^2 and 336×256 pixels with 607 nm pixels. Image analysis algorithms coded in FORTRAN were used to track colloid lateral motion with sub-pixel resolution[56] and to integrate the evanescent wave scattering intensity from each colloid (where absolute particle-wall separation is determined by h-$h_{ref}=\beta^{-1}\ln(I_{ref}/I)$,[19] see Fig. 1).[21]

Equilibrium Analysis. TIRM was used to measure the 3D trajectories of ~5-10 particles for 18 minutes at a frame period of τ=36ms (28 frame/s) to yield 3x10^4 images and coordinates for each particle. From the height coordinates of each particle, a height histogram, $p(h_i)$, was constructed for with bin sizes of 3 nm, which were normalized by the number of observations at the most probable height, $p(h_m)$. Single particle height histograms were averaged together to produce ensemble average height histograms.[21] By inverting single particle and average multi-particle histograms using Boltzmann's equation (Eq. (16)), TIRM measured each particle's average interactions with sampled surface locations and an ensemble particle−wall interaction averaged over all particles and surface positions. To account for experimental signal noise (laser, detector, etc.), theoretical potentials were convoluted with a Gaussian kernel with a standard deviation based on measuring the apparent height excursions of irreversibly deposited particles.[59]

Dynamic Analysis. A Bayesian Inference (BI) method was used to analyze TIRM measured particle normal trajectory data to obtain the Smoluchowski equation coefficients ((Eq. (19)), $D_\perp(h)$, $U(h)$). We previously implemented and described the BI method for analyzing TIRM measured interfacial colloidal trajectories[9] (and colloidal assembly trajectories[60]) in several material systems with and without interfacial macromolecules.[25, 29] These prior references contain implementation details,[9, 25, 29, 60] and the original theoretical development is reported elsewhere.[61] In brief, the analysis is based on a measured "jump matrix", $N(h_i, \tau | h_j, 0)$, which counts the number of jumps between all initial heights, h_j, and final heights, h_i, during an observation time, τ. Practically, TIRM trajectory data is obtained with τ=36ms (CCD camera frame period) for a total of 18 minutes and discretized into 3nm bins (same as equilibrium analysis). Then, for all trajectories passing through each initial height, h_j, the jump matrix records the relative statistical sampling of all subsequent heights, h_i, after a 36ms period. To mitigate statistical sampling limitations, the jump matrix was smoothed in less sampled bins (<40% of max count) by the same Gaussian kernel used to convolute equilibrium data.

The BI analysis is based on obtaining transition probabilities, $p(h, t | h_0, 0)$, that can be related to a rate matrix, R_{ij}, with elements indicating the probability rate from h_j to h_i. Analysis of the rate matrix yields the equilibrium probability of each height, $p(h_i)$ (see prior references for details[9, 61]).

As in the equilibrium analysis, $U(h)$ is related to $p(h_i)$ via Boltzmann's equation (Eq. (16)), and the diffusivity landscape is obtained as,

$$D\left[(h_i + h_{i+1})/2\right] = \Delta h^2 R_{i+1,i}\left[p(h_i)/p(h_{i+1})\right]^{1/2} \quad (20)$$

To obtain $p(h, t \mid h_0, 0)$, a likelihood function for the model parameters is defined as,

$$-\ln L = -\sum_k \sum_j \sum_i N(h_i, t_k \mid h_j, 0) \ln p(h_i, t_k \mid h_j, 0) \quad (21)$$

which describes the probability of the observed data, $N(h_i, t_k \mid h_j, 0)$, given the parameters of the model, $p(h_i, t_k \mid h_j, 0)$, based on Bayes' theorem. In practice, $-\ln L$ was minimized by varying model parameters via a Metropolis Monte Carlo algorithm (in FORTRAN; using a linear algebra package). In this work, $U(h)$ was fixed to the equilibrium solution to minimize uncertainty in $D_\perp(h)$. Convergence was determined when $-\ln L$ fluctuated within an equilibrated tolerance, and then $D_\perp(h)$ was obtained as the average of all converged models within the equilibrium fluctuations. Ensemble average $D_\perp(h)$ were obtained by averaging over all single particles. To smooth data at large separations with the most experimental noise and lower statistics, $D_\perp(h)$ profiles were re-binned to 15nm.

Results & Discussion

Bare Colloids & Surfaces: Interactions & Diffusion

Before investigating the role of adsorbed polymers on colloidal interactions and dynamics, we provide a baseline by first measuring and modeling bare particles near bare surfaces. Ensemble TIRM is used to measure the 3D Brownian motion of an ensemble of 2μm colloids electrostatically levitated over a glass microscope slide in aqueous 1mM NaCl (**Fig. 3**). The equilibrium height distribution for each particle is quantitatively close to the ensemble average, which indicates particles and microscope slide are chemically and physically uniform. Potential energy profiles are obtained by inverting measured height histograms using Boltzmann's equation (Eq. (16)). Measured kT-scale interactions are accurately modeled by superposition of electrostatic, van der Waals, and gravitational potentials (Eq. (1)). **Tables 1, 2** include parameters in potentials, which agree with TIRM and independent characterization methods within their respective uncertainties. The small spread of the individual potentials about the ensemble average on the gravitational potential are due to finite size polydispersity,[21] where the gravitational potential radius cubed dependence has a larger effect than colloid-surface potentials proportional to radius.

With an understanding of the equilibrium interaction potentials, we next analyze the same 3D particle trajectories to measure diffusion normal and parallel to the underlying planar surface. Using Bayesian inference (BI) to fit the Smoluchowski equation coefficients (Eq. (19)) to the measured colloidal dynamics normal to the substrate, we again obtain the same potential energy profile, $U(h)$, as the Boltzmann inversion (**Fig. 3C**) but now also obtain the position dependent diffusivity, $D(h)$ (**Fig. 3D**). In the BI analysis, we ultimately fix $U(h)$ to the result obtained from the equilibrium analysis, because it has less noise via the numerical features of that analysis, but the curves agree via both analyses within their uncertainties. The theoretical curve for the position dependent diffusivity based on hydrodynamic interactions (Eqs. (7)-(9)) is plotted by adjusting the absolute separation scale for the data (by determining each particle's most probable height h_m in Eqs. (15), (16)); values in **Table 2**). It should be noted the particle size used in the $D(h)$ theory is obtained sensitively *in situ* from the radius cubed dependence of the gravitational potential. The

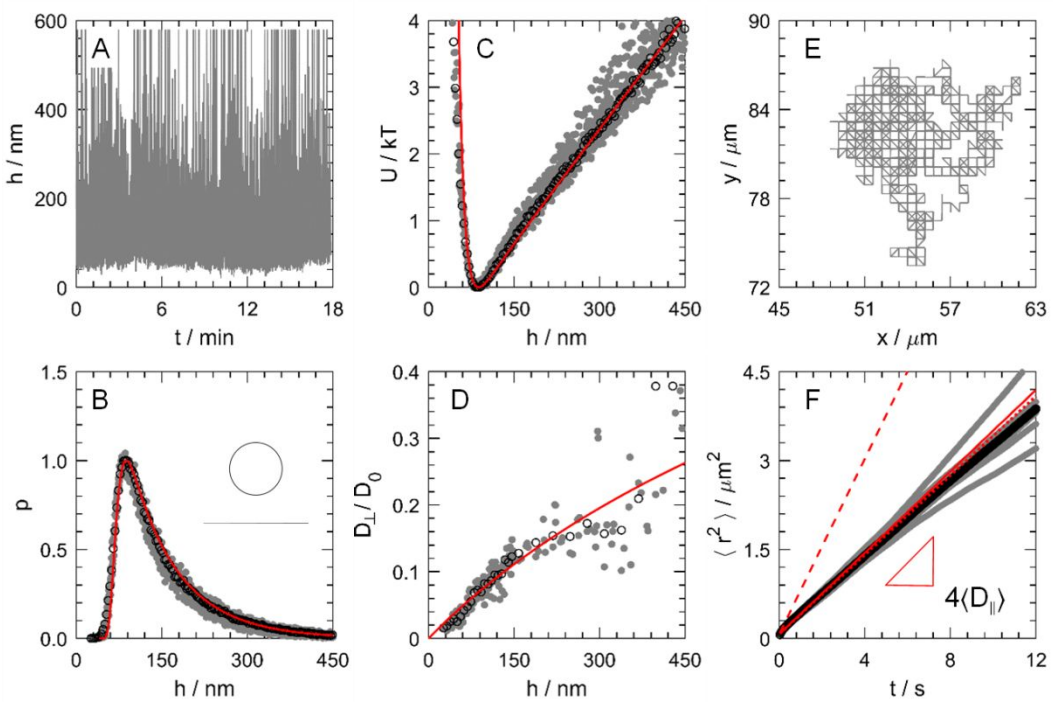

Fig 3. Interactions and diffusion of 7 bare silica colloids electrostatically stabilized over a bare glass surface. (A) Elevation trajectory, *h*, of single particle experiencing Brownian motion above a surface. (B) Histogram and (C) potential energy of single particles (grey) and their ensemble average (black) with theory (red, Eqs. (1), (15)) from superposition of gravitational, van der Waals, and electrostatic potentials (where $U/kT=U(h)-U(h_m)/kT$, and h_m is the most probable height; see Eq (16)). (D) Normal position dependent diffusivity of single particles and their ensemble average and theory (red, Eq. (8)). (E) 2D (x,y) trajectory of same single particle as panel A. (F) 2D mean squared displacement vs. time for single particles and their ensemble average and theory for Stokes-Einstein (dashed red) and averaged elevation dependent lateral diffusivity from the model (solid red, Eq. (14)) and from fit to the measurement (dotted red, Eq. (18)).

agreement between the measured and theoretical $D(h)$ is excellent within the limits of uncertainty of the BI method (and how it propagates error associated with decreasing signal to noise ratio with increasing particle elevation for evanescent wave scattering[9]).

Table 1. Energy and diffusivity landscape model global constants in Eqs. (1)-(19).

T [K]	ρ_p [kg m^{-3}][a]	ρ_m [kg m^{-3}][b]	g [m s^{-2}][c]	$\Psi_p = \Psi_w$ [mV][d]	A [kT nm^{p+1}][e]	p [1][e]	ϵ [1][f]	μ [mPa s][g]
293	1960	1000	9.807	-21± 3	12.75	2.154	78	1.01

[a]manufacturer reported silica particle density, [b]water density at 293 K,[62] [c]acceleration due to gravity, [d]electrostatic surface potentials fit to Eq. (3), [e]Eq. (4) parameters fit to Lifshitz theory for h>20nm,[21] [f]water dielectric constant at 293 K,[62] [g]water viscosity at 293 K[62]

Table 2. **Energy landscape model parameters in Eqs. (1)-(6).**
Cases correspond to analysis of data in Fig. 3 for bare, Fig. 4 for PEG-PEG, and Fig. 5 for PEG-mucin. For polymer mediated interactions in Eqs. (6)-(13), $2L_S$ is taken to be $L_{S,1}+L_{S,2}$, where $L_{S,1}=L_{S,2}$ for symmetric layers and different values are used for each layer in asymmetric interactions.

case	c_{NaCl} / mM[a]	κ^{-1} / nm[b]	$2a$ / nm[c]	h_m / nm[c]	$L_{S,1}$ / nm[d]	$L_{S,2}$ / nm[d]	Γ / kT[d]	γ^{-1} / nm[d]
bare	1	9.61	2097 ± 80	79 ± 9	-	-	-	-
PEG-PEG	150	0.785	2022 ± 18	33 ± 1	18 ± 2	18 ± 2	1984 ± 120	3.2 ± 0.4
PEG-mucin	150	0.785	2024 ± 14	90 ± 15	18 ± 2	214 ± 30	18.5 ± 4.5	41 ± 6

[a]as prepared and confirmed by solution conductivity, [b]computed from c_{NaCl} via Eq. (3), [c]ensemble average fit ± upper and low bounds for single particle fits

Table 3. **Diffusivity landscape model parameters in Eqs. (7)-(19).**
Cases are the same as in Table 2. Hydrodynamic layer thicknesses, L_H, and permeability parameter, n, are obtained by fitting Eq. (12) to measured $D_\perp(h)$ data. For polymer mediated hydrodynamic interactions in Eqs. (12) and (13), $2L_H$ is taken to be $L_{H,1}+L_{H,2}$, where $L_{H,1}=L_{H,2}$ for symmetric layers and different values are used for asymmetric interactions. Modeled $\langle D_\parallel \rangle$ are computed from Eq. (14), and measured $\langle D_\parallel \rangle$ are fit measurements via Eq. (18). The intercept of Eq. (18) provides an estimate of lateral resolution relative to the image pixel dimension (pixel size = 607 nm, see *Methods* for details).

case	$L_{H,1}$ / nm[a]	$L_{H,2}$ / nm[a]	n[b]	model $\langle D_\parallel \rangle / D_0$[c]	fit $\langle D_\parallel \rangle / D_0$[a]	fit Δ/μm[a]	Δ/pixel size
bare	-	-	-	0.43	0.42 ± 0.06	0.31 ± 0.01	0.51
PEG-PEG	12 ± 1	12 ± 1	1.0	0.37	0.37 ± 0.06	0.27 ± 0.02	0.44
PEG-mucin	12 ± 1	82 ± 1	1.0	0.42	0.40 ± 0.03	0.28 ± 0.01	0.46

[a]ensemble average fit ± upper and low bounds for single particle fits, [b]n<1 is aphysical, so 1 is chosen as a limiting minimum value, [c]computed using ensemble average values

After understanding colloidal interactions and diffusion normal to the wall, we measure from 3D trajectories the colloidal diffusion parallel to the underlying surface (**Figs. 3 E,F**). The 2D (x,y) trajectories of each particle is analyzed as the mean squared displacement vs. time using multiple time origins, and then each single-particle curve is averaged to give the ensemble average $\langle r^2 \rangle$ vs. t, where the slope is related to lateral diffusivity as $4\langle D_{||} \rangle$. The square root of the intercept, Δ, is less than the CCD camera pixel dimension consistent with sub-pixel tracking. The theoretical average diffusivity given by Eq. (14), which depends on the lateral hydrodynamic correction (Eq. (11)) and the interaction potential, either from the model (Eq. (1)) or the measurement (Eq. (16)), agrees with the measured diffusivity with no adjustable parameters (**Table 3,** other parameters determined from normal interaction in **Tables 1, 2**). Every particle's directly measured 3D colloidal trajectory was analyzed to yield interactions and diffusion perpendicular and parallel to a flat surface agree with theoretical models (*i.e.*, parameters in **Tables 1-3** agree with independent measures within limits of uncertainty). These results provide a unique demonstration of direct sensitive measurements, novel non-equilibrium analyses, and rigorous models that show excellent agreement without obvious discrepancies, which suggests few open questions or additional refinement of theory, at least within measurement uncertainty for bare silica colloids and surfaces.

Polymer Brush Coated Colloids & Surfaces: Interaction Potentials

Having validated the trajectory analysis and theoretical models for interactions and diffusion of bare colloids on bare surfaces, we next investigate colloids and surfaces interacting with adsorbed polymer brushes in physiological ionic strength media (**Fig. 4**). Adsorption of a PEG triblock onto hydrophobically modified silica colloids and glass surfaces, which is known to generate brush layer architectures, sterically stabilizes colloidal particles in 150 mM NaCl when electrostatic interactions are short range via screening.[9, 47, 59] The resulting steric stabilization is sufficiently robust that every single particle observed in microscopy experiments performs indefinite 3D Brownian motion above the planar substrate, indicating all particles and surface positions have uniform brush layers.

The histogram of heights sampled by each particle is noticeably narrower in the case of steric stabilization than electrostatic stabilization. Inversion of each particle's height histogram reveals particle-surface potential energy profiles indicating a short-range steric repulsion, a small ~1kT energy well (see **Fig. 4C** inset), and the same gravitational potential energy as the bare particles. The measured potentials are accurately modeled by the superposition of steric, van der Waals, and gravitational potentials (Eq. (1)), where electrostatic interactions are effectively screened so their inclusion produces a negligible contribution. Because the van der Waals potential

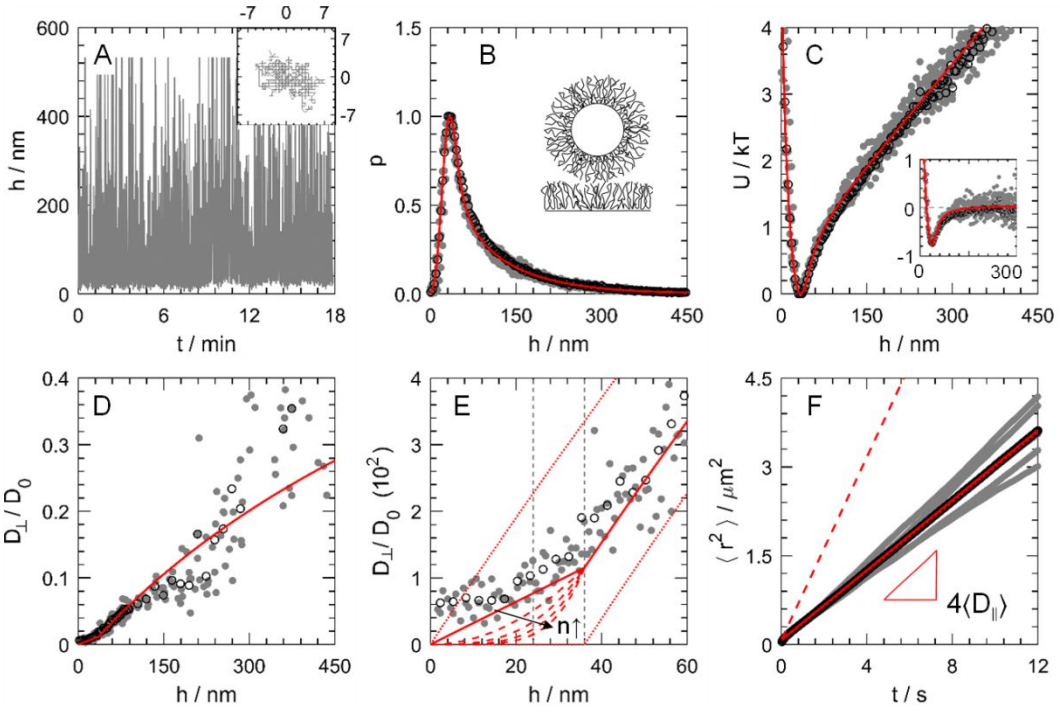

Fig. 4. Interactions and diffusion of 5 PEG brush coated colloids sterically stabilized over PEG brush coated surface. (A) Elevation trajectory, *h*, and 2D (x,y) trajectory (inset) of single particle experiencing Brownian motion above a surface. (B) Histogram and (C) potential energy of single particles (grey) and their ensemble average (black) with theory (red, Eqs. (1),(15)) from superposition of gravitational, van der Waals, and steric potentials. Inset shows same data/theory with gravity subtracted to show the normal potential well (D) Normal position dependent diffusivity of single particles and their ensemble average and theory (red, Eq. (8)). (E) Zoom view of diffusivity profile in panel D. Vertical lines indicate fit L_S and L_H. Final fit shown by solid red line. Dotted red lines indicate impermeable/permeable brush limits, and dashed red lines show varying value *n*-values to tune permeability profile inside brush, with an arrow indicating increasing *n*. (F) 2D mean squared displacement vs. time curves for single particles and their ensemble average and theory for Stokes-Einstein (dashed red) and averaged elevation dependent lateral diffusivity from the model (solid red, Eq. (14)) and from fit to the measurement (dotted red, Eq. (18)).

between the silica particle and glass substrate is well known,[21, 42, 47] it is used to determine the absolute separation scale without any adjustable parameters (**Table 2**).

The interaction of the PEG brushes is accurately modelled by the steric potential (Eq. (6)), including either the full form[31] or simple exponential form[29, 50] (that is accurate for the brush compression extent in the present measurements). We report the simple exponential form prefactor and decay length (**Table 2**), which can be directly related to the rigorous theory uncompressed layer free energy and layer thickness, also with no adjustable parameters (again within uncertainty of our measurements and independently measured parameters).[59] The PEG brush thickness on both the particle and wall surfaces is L_s=18 nm, and contact of two brush layers occurs at $2L_s$=36 nm. Because the onset of osmotic repulsion is measured directly, the uncertainty in the height approaches the spatial resolution limit of TIRM precision on the order of ~1nm. Ultimately, theories for the polymer brush repulsion and van der Waals attraction parameters accurately quantify the potential energy profile obtained from measured 3D colloidal trajectories.

Polymer Brush Coated Colloids & Surfaces: Interfacial Diffusion

We next measure diffusion normal and parallel to the wall for polymer coated colloids and

surfaces. To obtain the position dependent diffusivity normal to the substrate, $D_\perp(h)$, we use without modification the same non-equilibrium analysis used for bare particles and the same 3D particle trajectories interpreted as potential energy profiles in the equilibrium analysis. The resulting diffusivity landscapes (**Figs. 4D,E**) for each particle and the ensemble average decreases as surface separation decreases. The position dependence at large surface separations have a similar monotonically decreasing dependence for bare and polymer coated colloids and surfaces. At separations approaching brush contact, the measured diffusivity landscape vanishes with a different functionality than the bare particle asymptotic contact behavior.

Models for colloidal diffusivity landscapes (Eqs. (8), (9), (12)) in the presence of polymer brushes, including limiting trends, help understand some of the key features in the measured $D_\perp(h)$. For reference, a vertical line in **Fig. 4E** at h=2L_s=36nm indicates the onset of steric repulsion on the kT-scale from the measured potential energy profile (**Fig. 4C**). Plotting the $D_\perp(h)$ bare surface model (Eqs. (8), (9)) from h=0 (bare surface contact) corresponds to completely permeable brushes, and plotting the model from h=2L_s indicates completely impermeable brushes. These limits of completely permeable/impermeable layers fall above and below the measured data, which indicates an accurate model lies somewhere in between these cases. Shifting the bare surface model a distance 2L_H=24nm (**Table 3**) captures the long-range behavior of measured $D_\perp(h)$ to brush contact at h=2L_s=36nm. The apparent thinner brush hydrodynamic thickness is consistent with dynamic light scattering measurements of the same PEG brushes increasing apparent particle size via a decreased diffusivity, but also appearing thinner compared to steric layer thickness.[63] In short, shifting the effective hydrodynamic contact distance accounts reasonably well for hydrodynamic interactions at separations greater than brush contact.

The behavior of $D_\perp(h)$ for h<2L_s corresponds to separation where the brushes are being compressed and their permeability is expected to continuously change with compression. A more rigorous model for lubrication within compressed brushes,[41] which we have previously implemented and tested,[9] shows different functionalities depending on brush density profile and permeability models. However, this compressed brush lubrication model is complex and difficult to validate via independently testable parameters. Instead, we implement a minimally complex model that captures key features of the position dependent diffusivity for separations less than brush contact (Eq. (12)). The parameter "n" in Eq. (12) can tune the effective permeability profile. In **Fig. 4E**, we choose n=1 to capture the $D_\perp(h)$ trend for h<2L_s. Although apparent finite diffusivities appear to persist to substrate contact (h=0), these are likely an artifact of the BI analysis interpreting statistical noise due to limited sampling as finite diffusion (given their relatively high energies and reduced sampling on the potential energy profile). Our simple model for the separation dependence of the colloidal diffusion as the brush is compressed is necessary to explain in a consistent manner the particle Brownian motion that produces brush compression in the measured potential energy profile (**Fig. 4C**). Overall, the general features of the measured $D_\perp(h)$ are well captured by the simple model in Eq. (12).

With knowledge of interactions and diffusion normal to the underlying surface, we next analyze lateral diffusion from measured 3D particle trajectories of the polymer-coated particles over the polymer-coated surface. A representative lateral trajectory for a single polymer coated particle (**Fig. 4A**) shows unbiased Brownian motion over the entire 18-minute observation period, which covers a smaller spatial extent than a similar single bare particle ((~10 μm)^2 vs. (~15 μm)^2, **Fig. 3E**). Each single particle $\langle r^2 \rangle$ vs. t curve and their ensemble average are quantitatively similar at short times with slopes of 4$\langle D_{||} \rangle$ (**Table 3**). To model the average lateral diffusivity, we again

use Eq. (14) that includes the relative height distribution via Boltzmann sampling of the normal potential energy landscape and the elevation dependent lateral diffusivity based on hydrodynamic interactions. The theoretical average lateral diffusivity agrees with measured value within the uncertainty of the points in **Fig. 4**, which is smaller than the plotted point size. The same values of L_H and n are used as determined from the directly measured $D_\perp(h)$, so that no new adjustable parameters are introduced to obtain agreement between experiment and theory in **Fig. 4**.

The net effect of polymer brushes on lateral diffusivity is determined by competing effects that are averaged together (via the integral over the position dependent interactions in Eq. (14)). The polymer brush coated particle $\langle D_{||} \rangle$ is nearly ~10% less than the bare particle, which appears to indicate polymer layers impede diffusion. However, the position dependent correction in $D_{||}(h)$ (Eqs. (10)-(13)) that accounts for hydrodynamic interactions indicates a higher lateral diffusivity at the same elevation for a permeable layer compared to an impermeable layer. The source of the smaller $\langle D_{||} \rangle$ for brush coated particles compared to bare particles is the shape of the particle-wall potential energy profile that determines relative sampling of different elevations and their associated diffusivities. Practically, bare electrostatically levitated particles sample higher elevations on average than the brush coated particle with shorter range steric repulsion and a small amount of van der Waals attraction. As a result, bare particles have higher lateral diffusivities at higher elevations and thus higher average lateral diffusivities. In contrast, if particles with the same interaction potentials and permeable vs. impermeable brushes are compared, particles and surfaces with impermeable brushes produce slower lateral diffusion. Such effects account for only ~10% differences in lateral diffusivities but demonstrate the interplay of different interactions mediating polymer brush lubrication. Understanding effects of brush interactions on lateral diffusion together with the significant vanishing/diverging effects on normal diffusion indicates consistent mechanisms that determine lubrication between polymer brush coated colloids and surfaces.

Asymmetric PEG Brush Coated Colloids & Adsorbed Mucin Surfaces: Interactions & Diffusion

To understand asymmetric interactions between polymer brush coated colloids and biological barriers, as in biomedical applications, we next measure interactions of PEG brush coated colloids and adsorbed mucins (as a basic model of mucus barrier interfaces). Performing the same measurements and analysis of 3D colloidal trajectories as for bare and symmetric brush coated surfaces (**Figs. 3, 4**), similar plots of trajectory data, interactions, and diffusion are reported in **Fig. 5** for PEG brush coated colloids over adsorbed mucin surfaces. By adsorbing mucin to hydrophobically modified microscope slides in physiological ionic strength media (following literature methods and our previous work), the novel feature in these final studies is the formation of thick, porous mucin layers. The mucin itself has a bottlebrush architecture and adsorbed mucin layers are not brushes but likely have network structures.[64] By measuring interactions and diffusion of PEG brush coated colloids on adsorbed mucin layers we are able to infer a number of physical characteristics of the adsorbed mucin layers.

The potential energy profiles for each brush coated particle interacting with mucin layers (**Fig. 5C**) at different substrate positions are similar to each other and the ensemble average with similar uniformity to bare particle and symmetric PEG interactions (**Figs. 3C, 4C**). The consistency of measured potentials for every particle and surface position sampled by freely diffusing colloidal particles indicates chemical and physical uniformity of particles and adsorbed layers. The asymmetric PEG-mucin steric repulsion is long-range with a 41 nm decay length, which is >10x the decay length of the symmetric PEG brush interactions. We previously reported asymmetric brush steric potentials,[29, 50] which have a complex combined dependence on the

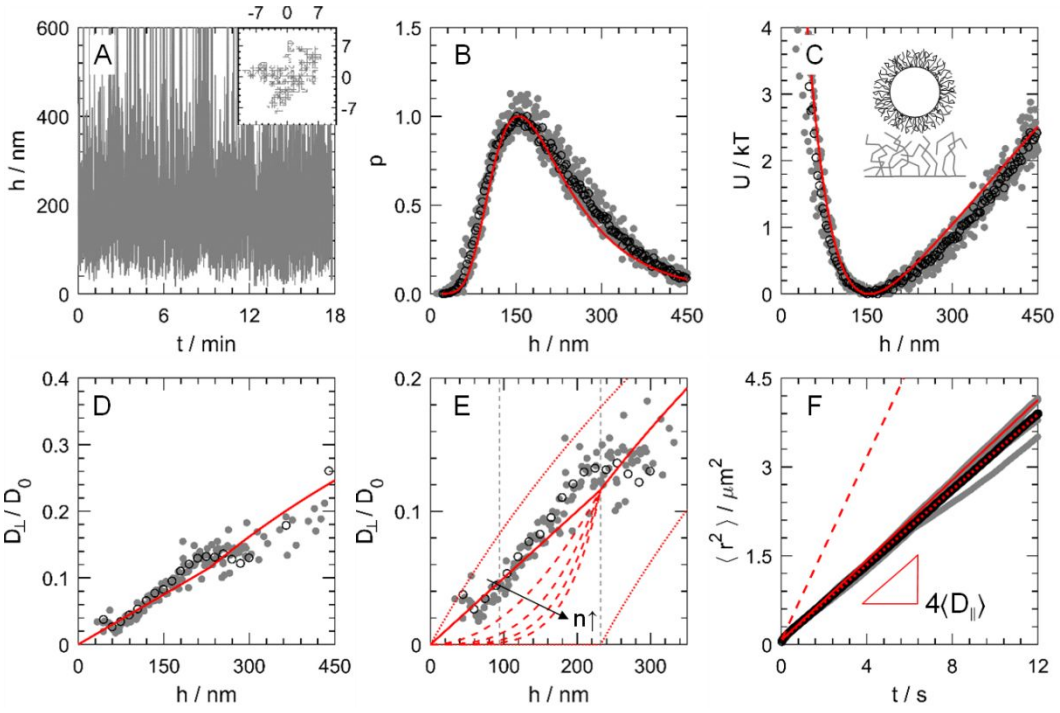

Fig 5. Interactions and diffusion of 5 PEG brush coated colloids sterically stabilized over adsorbed mucin coated surface. (A) Elevation trajectory, *h*, and 2D (x,y) trajectory (inset) of single particle experiencing Brownian motion above a surface. (B) Histogram and (C) potential energy of single particles (grey) and their ensemble average (black) with theory (red, Eqs. (1), (15)) from superposition of gravitational, van der Waals, and steric potentials. (D) Normal position dependent diffusivity of single particles and their ensemble average and theory (red, Eq. (8)). (E) Zoom view of diffusivity profile in panel D. Vertical lines indicate fit L_S and L_H values. Final fit shown by solid red line. Dotted red lines indicate impermeable/permeable brush limits, and dashed red lines show varying value *n*-values to tune permeability profile inside brush, with an arrow indicating increasing *n*. (F) 2D mean squared displacement vs. time curves for single particles and their ensemble average and theory for Stokes-Einstein (dashed red) and averaged elevation dependent lateral diffusivity from the model (solid red, Eq. (14)) and from fit to the measurement (dotted red, Eq. (18)).

uncompressed brush free energies and thicknesses. The adsorbed mucin is not expected to satisfy the assumptions of a brush architecture (grafting density, concentration profile, equation of state, etc.). As a result, although the steric interaction is well fit by an exponential repulsive potential, it is not straightforward to infer independent layer parameters from the model fit to the measured potential. However, because the steric repulsion is much longer range (onset of steric repulsion at $L_{S,1}+L_{S,2}$=232 nm, **Table 2**) compared to the symmetric PEG brush interactions, the adsorbed mucin appears to provide the dominant contribution to the decay length and net soft repulsion.

The mucin thickness is approximated from the absolute scattering intensity (intensity at steric repulsion onset, I_S, compared to deposited bare particle intensity, I_0, gives $L_{S,1}+L_{S,2}= \beta^{-1}\ln(I_0/I_S)$, as previously demonstrated[24, 29, 47]). This thickness is consistent with the absence of van der Waals attraction (and the diffusivity profile discussed in the following). The thickness measured in this study is also comparable to our prior TIRM measurements of symmetric mucin interactions (>200 nm).[29] The mucin dimensions are thicker than single layer dimensions inferred from hydrodynamic (~5-20nm)[65] and force (~70-80 nm)[66] measurements. However, the sensitivity of TIRM to the onset of weak macromolecular interactions is expected to occur at greater separations than these other measurements. In particular, strong compression will yield thinner

layer estimates, and flow through permeable layers will also yield a thinner hydrodynamic thickness. Measured mucin persistence lengths of 35 nm[67] can also be expected to give thick adsorbed mucin layer dimensions.

Measuring the normal position dependent diffusivity (**Fig. 5D,E**) and average lateral diffusivity (**Fig. 5F**) provides a consistent interpretation of the adsorbed mucin role in hydrodynamic interactions. We fit the measured $D_{\perp}(h)$ data to Eq. (12) using a hydrodynamic contact value as $L_{H,1}+L_{H,2}$=94 nm, steric contact value as 232nm, and permeability profile parameter is again well represented using n=1.0. The measured $D_{\perp}(h)$ data is lies below the prediction for completely permeable layers (upper bound in **Fig. 5E**) but is also well above the impermeable layer limit (lower bound in **Fig. 5E**). The value of $D_{\perp}(h)$ is much higher at layer contact for the PEG brush-mucin than the symmetric PEG brush contact value. Our model does not distinguish independent PEG and mucin layer permeabilities (nor does any available model), but the relatively higher $D_{\perp}(h)$ data must be due to the mucin layer increased permeability dominating the overall lubrication during mucin compression. In short, the adsorbed mucin layer's high permeability produces a diffusivity landscape normal to the substrate that is not too different from the bare electrostatically stabilized particles and is quite different from the relatively less permeable PEG brush interactions.

Using the same hydrodynamic correction parameters in the model (Eqs. (10)-(14), **Table 3**) of the average lateral diffusivity $\langle D_{||} \rangle$ shows good agreement with the measurement (**Fig. 5F**). The adsorbed mucin layer produces the highest average lateral diffusivity of the three cases investigated in this work, even compared to the bare particle and surface. The mucin layer has a lower measured $D_{\perp}(h)$ curve and a lower modelled $D_{||}(h)$ curve (not shown but similar trends to $D_{\perp}(h)$ curves) compared to the bare surface curves on the separation scale between bare surfaces; this appears to contradict the higher $\langle D_{||} \rangle$ in the adsorbed mucin case. However, the PEG brush coated particle interacting with the adsorbed mucin layer produces higher diffusivities on the separation scale relative to contact (steric layer contact vs. bare surface contact), which produces a higher lateral diffusivity. Alternatively, this result can also be understood as averaging elevation dependent diffusivities by the relative sampling of each elevation (via Eq. (14)), where the PEG brush coated particle over mucin has higher diffusivities on average for the elevations it samples compared to the bare particle and surface case. The net result of the balance of steric and hydrodynamic interactions is a higher average diffusivity resulting from diffusion on a highly permeable mucin layer. These results demonstrate the net lubricating effect of a mucin layer, which may have relevance to designing and optimizing particle coating to mediate their interactions with mucus barriers in biomedical applications.

Conclusions

We report novel methods to measure, analyze, and model the 3D diffusion of colloids on interfaces both for bare surfaces and surfaces with different adsorbed macromolecules. The 3D colloidal trajectories are measured with nanometer scale resolution perpendicular to planar surfaces via TIRM and with sub-diffraction limit resolution parallel to surfaces via standard particle tracking methods. For diffusion perpendicular to surfaces, a time-averaged equilibrium analysis (Boltzmann inversion) provides a sensitive measure of colloidal interactions including electrostatic, van der Waals, and steric interactions. A dynamic analysis of colloidal trajectories, in addition to capturing colloidal interactions (due to conservative forces), also reveals the position dependent diffusivity due to hydrodynamic interactions. Standard analysis of lateral mean squared

displacement vs. time captures average diffusivities parallel to surfaces. Minimally complex models were developed to capture measured interactions and diffusion, which show excellent agreement within resolution limits in all cases with minimal adjustable parameters.

When comparing our results for bare, symmetric brush coated surfaces, and asymmetric brush-mucin interactions, several key findings emerge that clarify the role of adsorbed polymers in mediating colloidal interactions and diffusion. Position dependent interaction potentials, or energy landscapes, are well described by established rigorous interaction potentials including simplified functional forms reported in this work. The *kT*- and nanometer- scale sensitivity of the reported measurements of brush and van der Waals interactions demonstrate the simplest models that are sufficiently rigorous to capture interactions important to stability, diffusion, and transport.

Our results demonstrate established models for hydrodynamic interactions between bare particles and surfaces accurately capture 3D trajectory data. This finding is enabled by a dynamic trajectory analysis for diffusion normal to interfaces and models accounting for the interactions that determine relative sampling of different elevations for diffusion parallel to interfaces. Our measurements and models of diffusion normal and parallel to interfaces are based on consistent analysis and modeling of adsorbed polymer permeability under weak compression. The directly measured diffusivity profiles in the presence of interacting brushes and adsorbed mucin indicate the role of permeability profiles within adsorbed layers that mediate lubrication while layers simultaneously undergo *kT*-scale compression. Average lateral particle diffusivities are about half their bulk values. However, permeable brushes alter normal diffusivities near contact to produce finite values compared to vanishing bare particle contact diffusivities, which demonstrates the non-trivial nature of brush lubrication on colloidal diffusion. Ultimately, our measurements and models demonstrate how colloidal interactions and diffusion near surfaces are modified by adsorbed polymers, which can be used to design and optimize polymer coatings for diverse applications.

Data availability

Data for this paper including raw videos (*.seq* files), custom analysis codes (FORTRAN and MatLab) and analyzed values (*.txt* files) are available at https://doi.org/10.7281/T1/RPCQP5.

Conflicts of interest

There are no conflicts to declare.

Acknowledgments

We acknowledge financial support by the National Science Foundation 2104499 and the donors of ACS Petroleum Research Fund under 62378-ND9.

References

1. Smay, J. E.; Cesarano, J.; Lewis, J. A. Colloidal Inks for Directed Assembly of 3-D Periodic Structures. *Langmuir* **2002,** *18*, 5429-5437.
2. Arpin, K. A.; Mihi, A.; Johnson, H. T.; Baca, A. J.; Rogers, J. A.; Lewis, J. A.; Braun, P. V. Multidimensional Architectures for Functional Optical Devices. *Adv. Mater.* **2010,** *22*, 1084-1101.
3. Ryan, J. N.; Elimelech, M. Colloid Mobilization and Transport in Groundwater. *Colloids and Surfaces A: Physicochemical and Engineering Aspects* **1996,** *107*, 1-56.
4. Mitchell, M. J.; Billingsley, M. M.; Haley, R. M.; Wechsler, M. E.; Peppas, N. A.; Langer, R. Engineering Precision Nanoparticles for Drug Delivery. *Nature Reviews Drug Discovery* **2021,** *20*, 101-124.

5. Russel, W. B.; Saville, D. A.; Schowalter, W. R. *Colloidal Dispersions*. Cambridge University Press: New York, **1989**.
6. Brenner, H. The Slow Motion of a Sphere through a Viscous Fluid Towards a Plane Surface. *Chem. Eng. Sci.* **1961,** *16*, 242-251.
7. Goldman, A. J.; Cox, R. G.; Brenner, H. Slow Viscous Motion of a Sphere Parallel to a Plane Wall -- I. Motion through a Quiescent Fluid. *Chem. Engr. Sci.* **1967,** *22*, 637-651.
8. Beltran-Villegas, D. J.; Sehgal, R. M.; Maroudas, D.; Ford, D. M.; Bevan, M. A. Fokker–Planck Analysis of Separation Dependent Potentials and Diffusion Coefficients in Simulated Microscopy Experiments. *J. Chem. Phys.* **2010,** *132*, 044707.
9. Beltran-Villegas, D. J.; Edwards, T. D.; Bevan, M. A. Self-Consistent Colloidal Energy and Diffusivity Landscapes in Macromolecular Solutions. *Langmuir* **2013,** *29*, 12337-12341.
10. Israelachvilli, J. *Intermolecular and Surface Forces*. 3rd ed.; Academic Press: New York, **2011**.
11. Butt, H.-J.; Cappella, B.; Kappl, M. Force Measurements with the Atomic Force Microscope: Technique, Interpretation and Applications. *Surface Science Reports* **2005,** *59*, 1-152.
12. Klein, J.; Kamiyama, Y.; Yoshizawa, H.; Israelachvili, J. N.; Fredrickson, G. H.; Pincus, P.; Fetters, L. J. Lubrication Forces between Surfaces Bearing Polymer Brushes. *Macromolecules* **1993,** *26*, 5552-5560.
13. Dhinojwala, A.; Granick, S. Surface Forces in the Tapping Mode: Solvent Permeability and Hydrodynamic Thickness of Adsorbed Polymer Brushes. *Macromolecules* **1997,** *30*, 1079-1085.
14. Farida, B.; Diethelm, J. Hydrodynamics of Particle–Wall Interaction in Colloidal Probe Experiments: Comparison of Vertical and Lateral Motion. *Journal of Physics: Condensed Matter* **2003,** *15*, 3003.
15. McLean, S. C.; Lioe, H.; Meagher, L.; Craig, V. S. J.; Gee, M. L. Atomic Force Microscopy Study of the Interaction between Adsorbed Poly(Ethylene Oxide) Layers: Effects of Surface Modification and Approach Velocity. *Langmuir* **2005,** *21*, 2199-2208.
16. Raviv, U.; Frey, J.; Sak, R.; Laurat, P.; Tadmor, R.; Klein, J. Properties and Interactions of Physigrafted End-Functionalized Poly(Ethylene Glycol) Layers. *Langmuir* **2002,** *18*, 7482-7495.
17. Zappone, B.; Ruths, M.; Greene, G. W.; Jay, G. D.; Israelachvili, J. N. Adsorption, Lubrication, and Wear of Lubricin on Model Surfaces: Polymer Brush-Like Behavior of a Glycoprotein. *Biophysical Journal* **2007,** *92*, 1693-1708.
18. Ramakrishna, S. N.; Espinosa-Marzal, R. M.; Naik, V. V.; Nalam, P. C.; Spencer, N. D. Adhesion and Friction Properties of Polymer Brushes on Rough Surfaces: A Gradient Approach. *Langmuir* **2013,** *29*, 15251-15259.
19. Prieve, D. C. Measurement of Colloidal Forces with Tirm. *Adv. Colloid Interface Sci.* **1999,** *82*, 93-125.
20. Gong, X.; Wang, Z.; Ngai, T. Direct Measurements of Particle–Surface Interactions in Aqueous Solutions with Total Internal Reflection Microscopy. *Chemical Communications* **2014,** *50*, 6556-6570.
21. Wu, H.-J.; Bevan, M. A. Direct Measurement of Single and Ensemble Average Particle-Surface Potential Energy Profiles. *Langmuir* **2005,** *21*, 1244-1254.
22. Wu, H.-J.; Pangburn, T. O.; Beckham, R. E.; Bevan, M. A. Measurement and Interpretation of Particle−Particle and Particle−Wall Interactions in Levitated Colloidal Ensembles. *Langmuir* **2005,** *21*, 9879-9888.
23. Frej, N. A.; Prieve, D. C. Hindered Diffusion of a Single Sphere Very near a Wall in a Nonuniform Force Field. *J. Chem. Phys.* **1993,** *98*, 7552-7564.
24. Bevan, M. A.; Prieve, D. C. Hindered Diffusion of Colloidal Particles Very near to a Wall: Revisited. *J. Chem. Phys.* **2000,** *113*, 1228-1236.
25. Bitter, J. L.; Duncan, G. A.; Beltran-Villegas, D. J.; Fairbrother, D. H.; Bevan, M. A. Anomalous Silica Colloid Stability and Gel Layer Mediated Interactions. *Langmuir* **2013,** *29*, 8835-8844.
26. Matse, M.; Chubynsky, M. V.; Bechhoefer, J. Test of the Diffusing-Diffusivity Mechanism Using near-Wall Colloidal Dynamics. *Physical Review E* **2017,** *96*, 042604.
27. Lavaud, M.; Salez, T.; Louyer, Y.; Amarouchene, Y. Stochastic Inference of Surface-Induced Effects

Using Brownian Motion. *Physical Review Research* **2021,** *3*, L032011.
28. Rivera-Morán, J. A.; Lang, P. R. Analysing Sources of Error in Total Internal Reflection Microscopy (Tirm) Experiments and Data Analysis. *Polymers* **2023,** *15*, 4208.
29. Swavola, J. C.; Edwards, T. D.; Bevan, M. A. Direct Measurement of Macromolecule-Coated Colloid–Mucus Interactions. *Langmuir* **2015,** *31*, 9076-9085.
30. de Gennes, P. G. Polymers at an Interface; a Simplified View. *Advances in Colloid and Interface Science* **1987,** *27*, 189-209.
31. Milner, T.; Witten, T. A.; Cates, M. E. Theory of the Grafted Polymer Brush. *Macromolecules* **1988,** *21*, 2610-2619.
32. Zhulina, E. B.; Borisov, O. V.; Priamitsyn, V. A. Theory of Steric Stabilization of Colloid Dispersions by Grafted Polymers. *Journal of Colloid and Interface Science* **1990,** *137*, 495-511.
33. Kreer, T.; Balko, S. M. Scaling Theory for Compressed Polymer-Brush Bilayers. *ACS Macro Letters* **2013,** *2*, 944-947.
34. Anekal, S.; Bevan, M. A. Self Diffusion in Sub-Monolayer Colloidal Fluids near a Wall. *J. Chem. Phys.* **2006,** *125*, 034906.
35. Grest, G. S. Normal and Shear Forces between Polymer Brushes. In *Polymers in Confined Environments*, Granick, S.; Binder, K.; de Gennes, P. G.; Giannelis, E. P.; Grest, G. S.; Hervet, H.; Krishnamoorti, R.; Léger, L.; Manias, E.; Raphaël, E.; Wang, S. Q., Eds. Springer Berlin Heidelberg: Berlin, Heidelberg, **1999**, pp 149-183.
36. Kreer, T. Polymer-Brush Lubrication: A Review of Recent Theoretical Advances. *Soft Matter* **2016,** *12*, 3479-3501.
37. Kjellander, R.; Florin, E. Water Structure and Changes in Thermal Stability of the System Poly(Ethylene Oxide)-Water. *J. Chem. Soc., Faraday Trans. I* **1981,** *77*, 2053-2077.
38. Wang, R. L. C.; Jürgen Kreuzer, H.; Grunze, M. The Interaction of Oligo(Ethylene Oxide) with Water: A Quantum Mechanical Study. *Physical Chemistry Chemical Physics* **2000,** *2*, 3613-3622.
39. Fredrickson, G. H.; Pincus, P. Drainage of Compressed Polymer Layers: Dynamics of a "Squeezed Sponge". *Langmuir* **1991,** *7*, 786-795.
40. Solomentsev, Y.; Kotov, A.; Starov, V. Hydrodynamical Interaction of Two Particles Covered with a Porous Layer. *International Journal of Multiphase Flow* **1992,** *18*, 739-750.
41. Potanin, A. A.; Russel, W. B. Hydordynamic Interaction of Particles with Grafted Polymer Brushes and Applications to Rheology of Colloidal Dispersions. *Phys. Rev. E* **1995,** *52*, 730-737.
42. Bevan, M. A.; Prieve, D. C. Direct Measurement of Retarded Van Der Waals Attraction. *Langmuir* **1999,** *15*, 7925-7936.
43. White, L. R. On the Derjaguin Approximation for the Interaction of Macrobodies. *Journal of Colloid and Interface Science* **1983,** *95*, 286-288.
44. Bike, S. G.; Prieve, D. C. Measurements of Double-Layer Repulsion for Slightly Overlapping Counterion Clouds. *Int. J. Multiphase Flow* **1990,** *16*, 727-740.
45. Prieve, D. C.; Russel, W. B. Simplified Predictions of Hamaker Constants from Lifshitz Theory. *J. Coll. Interfac. Sci.* **1988,** *125*, 1.
46. Pailthorpe, B. A.; Russel, W. B. The Retarded Van Der Waals Interaction between Spheres. *J. Colloid Interface Sci.* **1982,** *89*, 563-566.
47. Bevan, M. A.; Prieve, D. C. Forces and Hydrodynamic Interactions between Polystyrene Surfaces with Adsorbed Peo-Ppo-Peo. *Langmuir* **2000,** *16*, 9274-9281.
48. Bevan, M. A.; Petris, S. N.; Chan, D. Y. C. Solvent Quality Dependent Continuum Van Der Waals Attraction and Phase Behavior for Colloids Bearing Nonuniform Adsorbed Polymer Layers. *Langmuir* **2002,** *18*, 7845-7852.
49. Milner, S. T. Compressing Polymer Brushes - a Quantitative Comparison of Theory and Experiment. *Europhysics Letters* **1988,** *7*, 695-699.
50. Eichmann, S. L.; Meric, G.; Swavola, J. C.; Bevan, M. A. Diffusing Colloidal Probes of Protein–Carbohydrate Interactions. *Langmuir* **2013,** *29*, 2299-2310.
51. Einstein, A. Über Die Von Der Molekularkinetischen Theorie Der Wärme Geforderte Bewegung Von

in Ruhenden Flüssigkeiten Suspendierten Teilchen. *Annalen der Physik* **1905,** *17*, 549–560.
52. Chandrasekhar, S. Stochastic Problems in Physics and Astronomy. *Rev. Mod. Phys.* **1943,** *15*, 1-89.
53. Pawar, Y.; Anderson, J. L. Hindered Diffusion in Slit Pores: An Analytical Result. *Ind. Eng. Chem. Res.* **1993,** *32*, 743-746.
54. Happel, J.; Brenner, H. *Low Reynolds Number Hydrodynamics*. Prentice-Hall: Englewood Cliffs, NJ, **1965**.
55. Anderson, J. L.; Solomentsev, Y. Hydrodynamic Eeffects of Surface Layers on Colloidal Particles. *Chemical Engineering Communications* **1996,** *148-150*, 291-314.
56. Crocker, J. C.; Grier, D. G. Methods of Digital Video Microscopy for Colloidal Studies. *J. Colloid. Interface Sci.* **1996,** *179*, 298-310.
57. Savin, T.; Doyle, P. S. Static and Dynamic Errors in Particle Tracking Microrheology. *Biophys. J.* **2005,** *88*, 623-638.
58. van Helden, A. K.; Jansen, J. W.; Vrij, A. Preparation and Characterization of Spherical Monodisperse Silica Dispersions in Non-Aqueous Solvents. *J. Coll. Interfac. Sci.* **1981,** *81*, 354-368.
59. Petroff, M. G.; Garcia, E. A.; Dengler, R. A.; Herrera-Alonso, M.; Bevan, M. A. Kt-Scale Interactions and Stability of Colloids with Adsorbed Zwitterionic and Ethylene Oxide Copolymers. *Macromolecules* **2018,** *51*, 9156-9164.
60. Beltran-Villegas, D. J.; Sehgal, R. M.; Maroudas, D.; Ford, D. M.; Bevan, M. A. Colloidal Cluster Crystallization Dynamics. *J. Chem. Phys.* **2012,** *137*, 134901.
61. Hummer, G. Position-Dependent Diffusion Coefficients and Free Energies from Bayesian Analysis of Equilibrium and Replica Molecular Dynamics Simulations. *New J. Phys.* **2005,** *7*, 34.
62. Lide, D. R. *Crc Handbook of Chemistry and Physics*. CRC Press: New York, **2000**; Vol. 80.
63. Min, G. K.; Bevan, M. A.; Prieve, D. C.; Patterson, G. D. Light Scattering Characterization of Polystyrene Latex with and without Adsorbed Polymer. *Colloids and Surfaces A: Physicochemical and Engineering Aspects* **2002,** *202*, 9-21.
64. Joyner, K.; Song, D.; Hawkins, R. F.; Silcott, R. D.; Duncan, G. A. A Rational Approach to Form Disulfide Linked Mucin Hydrogels. *Soft Matter* **2019,** *15*, 9632-9639.
65. Shi, L.; Caldwell, K. D. Mucin Adsorption to Hydrophobic Surfaces. *Journal of Colloid and Interface Science* **2000,** *224*, 372-381.
66. Malmsten, M.; Blomberg, E.; Claesson, P.; Carlstedt, I.; Ljusegren, I. Mucin Layers on Hydrophobic Surfaces Studied with Ellipsometry and Surface Force Measurements. *Journal of Colloid and Interface Science* **1992,** *151*, 579-590.
67. Round, A. N.; Berry, M.; McMaster, T. J.; Stoll, S.; Gowers, D.; Corfield, A. P.; Miles, M. J. Heterogeneity and Persistence Length in Human Ocular Mucins. *Biophys. J.* **2002,** *83*, 1661-1670.

Direct Measurements & Simplified Models of Colloidal Interactions & Diffusion with Adsorbed Macromolecules

Mikael O. Ellingson and Michael A. Bevan†
Chemical & Biomolecular Engr., Johns Hopkins Univ., Baltimore, MD 21218

Data Availability Statement

Data for this paper, including: raw videos (*.seq* files), custom analysis codes (FORTRAN and MatLab) and analyzed values (*.txt* files) are available at https://doi.org/10.7281/T1/RPCQP5.

† To whom correspondence should be addressed. email: mabevan@jhu.edu